Eur. Phys. J. C (2023) 83:858
https://doi.org/10.1140/epjc/s10052-023-12041-5

THE EUROPEAN PHYSICAL JOURNAL C

Regular Article - Theoretical Physics

Properties of color-flavor locked matter in a quasiparticle model

Peng-Cheng Chu[1,a], **Qian Cao**[2], **He Liu**[1,b], **Xiao-Hua Li**[3,4,c], **Min Ju**[5,d], **Xu-Hao Wu**[6,e], **Ying Zhou**[7,f]

[1] The Research Center for Theoretical Physics, Science School, Qingdao University of Technology, Qingdao 266033, China
[2] School of Information and Control Engineering, Qingdao University of Technology, Qingdao 266033, China
[3] School of Nuclear Science and Technology, University of South China, Hengyang 421001, China
[4] Cooperative Innovation Center for Nuclear Fuel Cycle Technology and Equipment, University of South China, Hengyang 421001, China
[5] College of Science, China University of Petroleum (East China), Qingdao 266580, China
[6] School of Science, Yanshan University, Qinhuangdao 066004, China
[7] School of Physical Science and Technology, Inner Mongolia University, Hohhot 010021, China

Received: 15 May 2023 / Accepted: 14 September 2023 / Published online: 25 September 2023

Abstract We investigate the thermodynamical properties of color-flavor locked (CFL) quark matter at zero temperature, finite temperature, and strong magnetic field by using quasiparticle model. We find that considering CFL quark phase can significantly change the equation of state (EOS) as well as the properties of quark matter in quark stars (QSs) at finite temperature or under magnetic field within quasiparticle model. In particular, our results have shown that we can provide the large QSs within CFL quark phase from quasiparticle model by satisfying both the upper limit of $\Lambda_{1.4} < 800$ for the low-spin priors of 1.4 solar mass pulsars from GW170817 and the new estimates of the mass-radius region from PSR J0740 + 6620, PSR J0030 + 0451, HESS J1731-347, and 4U 1702-429, which cannot be obtained by considering the QSs with SQM within quasiparticle model.

1 Introduction

The properties of the star matter in the inner core of compact stars are considered as an important issue in nuclear physics and astrophysics [1–4]. In the results of recent pulsar observations, a number of massive compact stars have been detected and set rigid constraints on the equation of state (EOS) of strongly interacting matter. For instance, the radio pulsar PSR J1614-2230 [5] was precisely measured to be $1.97 \pm 0.04\ M_\odot$ by using the general relativistic Shapiro delay 12 years ago, and a new pulsar PSR J0348+0432 was found in 2013 with a mass of $2.01 \pm 0.04\ M_\odot$ [6]. In 2019, the authors of Ref. [7] use the data of relativistic Shapiro delay with the Green Bank Telescope to announce PSR J0740+6620 ($2.14^{+0.10}_{-0.09}\ M_\odot$ with 68.3% credibility interval and $2.14^{+0.20}_{-0.18}\ M_\odot$ with 95.4% credibility interval) as the most massive precisely observed pulsar, while in 2021 this star mass have been further updated as $2.08 \pm 0.07\ M_\odot$ [8,9]. The direct detection of the gravitational wave signal GW190817 from a binary compact star system has been reported by the LIGO-Virgo collaboration, and the upper limit of the tidal deformability of the $1.4\ M_\odot$ compact stars is set as $\Lambda_{1.4} < 800$ for the low-spin priors [10], which gives the new limitations on the properties of the nuclear matter symmetry energy and EOSs of strongly interacting matter. In 2020, the LIGO/Virgo Collaborations declare the mass of the secondary component m_2 of the newly discovered compact binary merger GW190814 [11] may reach $2.50\ M_\odot - 2.67\ M_\odot$ at 90% credible level, which sets very strict constraints on the EOS of strongly interacting matter if we considered the candidate of the secondary component of GW190814 as a compact star. In general, compact stars usually include neutron star (NS), quark star (QS), and hybrid star (HS). Neutron star matter is consisted with large fraction neutron and small fraction proton, and the star matter is considered as charge neutrality with a very tiny density of electrons. In the inner core of NSs, the hyperon, meson condensations, and even the absolutely stable strange quark matter (SQM) may appear, which implies NSs could be converted to QSs. The possible existence of QSs is still one of the most important fields of modern nuclear physics and astrophysics [12–24]. If one considered the supermassive compact stars as QSs, the observations may rule out some of

[a] e-mail: kyois@126.com (corresponding author)
[b] e-mail: liuhe@qut.edu.cn
[c] e-mail: lixiaohuaphysics@126.com
[d] e-mail: jumin@upc.edu.cn
[e] e-mail: wuhaoysu@ysu.edu.cn
[f] e-mail: yingzhow@163.com

the conventional phenomenological models of quark matter, whereas there still exist some other models which are able to produce massive quark star cases with strong isospin interaction inside the star matter [25–34]. It can be found that the EOS of the quark star matter in their descriptions becomes very stiff so as to support such massive quark stars.

On the other hand, for the more stable matter state of quarks than SQM, the color-flavor locked (CFL) state is considered as the most symmetric pairing state, where all the quark flavors and colors are paired [35–37]. As predicted, the quark matter in CFL phase might appear inside the compact stars (strange stars or the inner core of hybrid stars) [38,39]. If one considered describing QSs under CFL phase, the CFL quark matter in QSs should be made up of u, d, and s quarks with no electrons because of the charge neutrality in QSs, which means the fraction of u, d, and s quarks is identical. Hence the CFL quark matter represents the most symmetric pairing state for u, d, and s quark matter and might be more stable than normal nuclear matter [40,41].

This paper is organized as follows. We first investigate the thermodynamical properties of color-flavor locked quark matter at zero temperature, finite temperature, and strong magnetic fields. Then we calculate the properties of quark star at zero temperature and finite temperature with CFL quark matter by using quasiparticle model.

2 The theoretical formulism

2.1 Properties of SQM

From Farhi and Jaffe's research [16], SQM is absolutely stable and composed of u, d, and s quarks and leptons (e and μ), where the electric charge neutrality of SQM can be expressed as

$$\frac{2}{3}n_u = \frac{1}{3}n_d + \frac{1}{3}n_s + n_e. \tag{1}$$

For the quarks and leptons in SQM, the weak beta-equilibrium condition of SQM should also be considered as

$$\mu_d = \mu_s = \mu_u + \mu_e, \quad \text{and} \quad \mu_\mu = \mu_e. \tag{2}$$

Since color-flavor-locked (CFL) quark matter is predicted to be more stable than SQM, we study the equation of state (EOS) in next subsections to obtain the thermodynamical properties of CFL matter.

2.2 Properties of CFL matter at zero temperature

The CFL phase of quark matter is neutralized automatically with no leptons being considered in [38], which indicates that the baryon density of u, d, and s quarks is equal. The number density of each flavors of quarks at zero temperature can be given as

$$n_q = \frac{{k_f}^3}{\pi^2} + \frac{2\Delta^2\mu}{\pi^2}, \tag{3}$$

where k_f is Fermi momentum for quarks, and Δ means the nonvanishing common energy gap for different flavors of quarks. μ is the mean chemical potential for the quark matter in CFL phase, which is written as

$$\mu = \frac{1}{3}\sum_{i=u,d,s}\mu_i = \frac{1}{3}\sum_i\sqrt{{k_f}^2 + m_i^2}. \tag{4}$$

Among the phenomenological quark models, density dependent quark mass models have been widely used in many works [42–77], while there still exist other works considering the vector-vector interaction in the Lagrangian density to obtain stiff EOS of quark star matter [78–90]. In this work, we employ quasiparticle model to calculate the thermodynamical properties of CFL matter, whose analytic expression can be obtained by considering one-loop self energy diagrams in the hard dense loop approximation as [91–94]

$$m_q = \frac{m_{q0}}{2} + \sqrt{\frac{m_{q0}^2}{4} + \frac{g^2\mu_q^2}{6\pi^2}}. \tag{5}$$

Here m_{q0} is the quark current mass, and g means the strongly interacting coupling constant which is considered as a free input parameter in the present work. For CFL phase matter at asymptotically high densities, the u and d quark current masses can be considered as zero, and the current mass for strange quark mass is set as $m_{s0} = 95$ MeV in this work for CFL quark matter.

Then we can derive the total thermodynamic potential density for CFL matter as

$$\Omega = \sum_{i=u,d,s}[\Omega_i + B_i(\mu_i)] + B_m - 3\frac{\Delta^2\mu^2}{\pi^2}, \tag{6}$$

where B_m means the negative vacuum pressure term for quark confinement [95]. Ω_i is written as

$$\Omega_i = -\frac{g_i}{48\pi^2}\left[\mu_i\sqrt{\mu_i^2 - m_i^2}(2\mu_i^2 - 5m_i^2) + 3m_i^4\ln\frac{\mu_i + \sqrt{\mu_i^2 - m_i^2}}{m_i}\right]. \tag{7}$$

$B_i(\mu_i)$ comes from the chemical potential dependence in the constituent quark mass, which can be obtained as

$$B_i(\mu_i) = -\int_{m_i}^{\mu_i}\frac{\partial\Omega_i}{\partial m_i}\frac{\partial m_i}{\partial\mu_i}\mathrm{d}\mu_i. \tag{8}$$

The total energy density can be derived as

$$\mathcal{E} = \sum_i (\Omega_i + B_i(\mu_i) + \mu_i n_i) + B_m - 3\frac{\Delta^2\mu^2}{\pi^2}, \tag{9}$$

where $g_i = 6$ is the degeneracy factor for quarks. Then the pressure P at zero temperature can be derived as

$$P = -\sum_i (\Omega_i + B_i(\mu_i)) - B_m + 3\frac{\Delta^2\mu^2}{\pi^2}. \tag{10}$$

2.3 Properties of CFL matter at finite temperature

The free-particle contribution for each flavor of quarks can be expressed analytically at finite temperature as

$$\Omega_i = -\frac{g_i T}{2\pi^2}\int_0^\infty \left[\ln\left(1+\mathrm{e}^{-\left(\sqrt{p^2+m_i^2}-\mu_i\right)/T}\right) + \ln(1+\mathrm{e}^{-(\sqrt{p^2+m_i^2}+\mu_i)/T}\right] p^2 \mathrm{d}p. \tag{11}$$

From the numerical results, we find the chemical potential μ for CFL quark matter with all the parameter sets exhibits larger values than 200 MeV when the baryon density is larger than the zero-pressure density, and the temperature cases we considered in this work are all smaller than the chemical potential μ. The energy gap can be considered to be temperature dependent by following the studies of superconductivity in SQM [39,96], which can be obtained as

$$\Delta^T = 2^{-1/3}\Delta\sqrt{1-\left(\frac{T}{T_c}\right)^2}, \tag{12}$$

where $T_c = 0.57\Delta$ comes from the critical temperature of the superconducting nuclear matter. Then the total free energy density $\mathcal{F}$ can be written as

$$\mathcal{F} = \sum_i (\Omega_i + B_i(\mu_i) + \mu_i n_i) - 3\frac{{\Delta^T}^2\mu^2}{\pi^2} + B_m. \tag{13}$$

And the entropy density can be calculated by considering

$$S = -\sum_i \frac{\partial\Omega_i}{\partial T}. \tag{14}$$

Using $\mathcal{F} = \mathcal{E} - TS$, one can obtain the energy density of CFL quark matter at finite temperature, and the thermodynamical self-consistency can also be checked by calculating the baryon density of the minimum free energy per baryon and the zero-pressure point.

2.4 Properties of MCFL matter under strong magnetic fields

In Refs. [97–99], the authors discuss the properties of the quark matter under magnetic color-flavor locked (MCFL) phase within Nambu–Jona–Lasinio (NJL) model. Their results indicate that the original non-vanishing energy gap Δ of the CFL phase should be split in two MCFL gaps (Δ_1 and Δ_H) when the magnetic field is considered. Furthermore, a third gap may become significant at extremely strong magnetic field, which is larger than 10^{19} G. In this work we only consider Δ_1 and Δ_H for the quark matter in MCFL phase, and the thermodynamical potential density can be derived from [100] as

$$\Omega_{MCFL} = \Omega_{charged} + \Omega_{neutral} - 3\frac{\Delta^{*2}\mu^2}{\pi^2}, \tag{15}$$

where $\Omega_{charged}$ and $\Omega_{neutral}$ are the contributions from the redefined charged quarks within NJL model [97,100]. The redefined charges of quarks can be listed as

u_r	u_g	u_b	d_r	d_g	d_b	s_r	s_g	s_b
0	1	1	−1	0	0	−1	0	0

, (16)

where r, g, b means the color degree of freedom of different flavors of quarks. $\Delta^* = \sqrt{({\Delta_1}^2 + 2\Delta_H^2)/3}$ is the effective energy gap of MCFL phase. In the previous works [97,100], the energy gap Δ_1 and Δ_H are formed by the neutral quark pairs and charged quark pairs, respectively. In this work, we use Δ^* to compare with the results with Δ in zero magnetic field CFL quark matter for convenience. Then the thermodynamical potential density for charged quarks under magnetic fields in MCFL phase within quasiparticle model can be written as

$$\Omega_i = -\sum_{\nu=0}^{\nu_{max}^i}\frac{g_i(|q_i|B)}{2\pi^2}\alpha_\nu\left\{\frac{1}{2}\mu_i\sqrt{{\mu_i}^2 - s_i(\nu,B)^2} - \frac{s_i(\nu,B)^2}{2}\ln\left(\frac{\mu_i+\sqrt{{\mu_i}^2 - s_i(\nu,B)^2}}{s_i(\nu,B)}\right)\right\}, \tag{17}$$

where $\alpha_\nu = 2 - \delta_{\nu,0}$ and $g_i = 2$ is the spin degree of degeneracy for MCFL phase. In this work, we assume the direction of magnetic field is set along z axis [101–103], and then the Fermi energy for quarks under magnetic fields at zero temperature becomes

$$\mu_i = \sqrt{{k_{F,\nu}^i}^2 + s_i(\nu,B)^2}, \tag{18}$$

where $s_i(\nu,B) = \sqrt{m_i^2 + 2\nu|q_i|B}$. The upper Landau level ν_{max} is constrained as

$$\nu_{max}^i \equiv \mathrm{int}\left[\frac{{\mu_i}^2 - m_i^2}{2|q_i|B}\right], \tag{19}$$

where int$[\cdots]$ means the integer function.

Furthermore, the total energy density $\mathcal{E}_{tot}$ of MCFL phase can be obtained as

$$\mathcal{E}_{tot} = \Omega_{MCFL} + \sum_i (B_i(\mu_i) + \mu_i n_i) + B_m + \frac{B^2}{2}. \quad (20)$$

For the uncharged quarks in the rotated representation, the analytic expression can be referred from the zero magnetic field case of CFL quark matter within quasiparticle model. Moreover, the pressure for MCFL quark matter becomes anisotropic due to the $\mathcal{O}(3)$ rotational symmetry for MCFL quark matter might be broken. Then the anisotropic pressures which is parallel to the magnetic field is defined as the longitudinal pressure $P_\parallel$, while the pressure which is perpendicular to the magnetic field is defined as the transverse pressure $P_\perp$ [104,105], whose analytic forms are written as

$$P_\parallel = \sum_i \mu_i n_i - \mathcal{E}_{tot}, \quad (21)$$

and

$$P_\perp = \sum_i \mu_i n_i - \mathcal{E}_{tot} + B^2 - MB. \quad (22)$$

Here $M = -\frac{\partial \Omega}{\partial B}$ is the system magnetization.

3 Results and discussions

3.1 Thermal dynamical properties of CFL matter

In this subsection, we study the strange quark matter and CFL quark matter by considering β-equilibrium condition (the β-equilibrium condition for SQM can be obtained from Eqs. (1) and (2)). For CFL quark matter, the fraction and chemical potential of leptons are zero, and the number density of u, d, and s quarks are identical to satisfy the charge neutrality. Then the β-equilibrium condition for CFL quark matter can be written as $\mu = \mu_u = \mu_d = \mu_s$.

In Fig. 1, we show the free energy per baryon F and the pressure P of SQM and CFL quark matter as functions of baryon density n_B at $T = 0$ and $T = 50$ MeV with $\Delta(\Delta^T) = 0,\ 50,\ 100$ MeV (SQM case can be considered as $\Delta = 0$ case here). The parameter set for quasiparticle model we use here is g-2 (g=2, $B_m^{1/4}$=141MeV), which can describe the massive pulsar PSR J0348+0432 (with a mass of $2.01 \pm 0.04\ M_\odot$) [6] as QSs in SQM case within quasiparticle model in [94]. One can find in Fig. 1 that the baryon density of the minimum free energy per baryon is exactly the zero-pressure point density in all cases, which satisfies the requirement of the thermodynamical self-consistency (for $T = 0$ case, the free energy per baryon is identical to the energy per baryon). It can also be seen in Fig. 1 that the values of the free energy per baryon decreases when the temperature increases from zero to 50 MeV, while the pressure increases with temperature for both SQM and CFL quark matter cases. Furthermore, one can find that the minimum free energy per baryon begins decreasing when the nonvanishing common gap Δ^T is introduced at different temperatures, and the minimum free energy per baryon becomes much smaller when we change $\Delta^T = 50$ MeV to $\Delta^T = 100$ MeV, which indicates the CFL quark matter is more stable than the ordinary SQM at both zero temperature and finite temperature cases. Moreover, we can also obtain that the zero-pressure density in g-2 case decreases with Δ^T, and the pressure at fixed baryon densities gets larger with Δ^T, which implies that we might describe heavier and larger QSs with CFL quark matter compared with the QSs with SQM.

In Fig. 2, we calculate the energy per baryon and pressure of SQM and CFL quark matter as functions of baryon density n_B under constant magnetic fields $B = 0$ and $B = 2 \times 10^{18}$G with $\Delta = 0,\ 50,\ 100$ MeV and $\Delta^* = 0,\ 50,\ 100$ MeV.

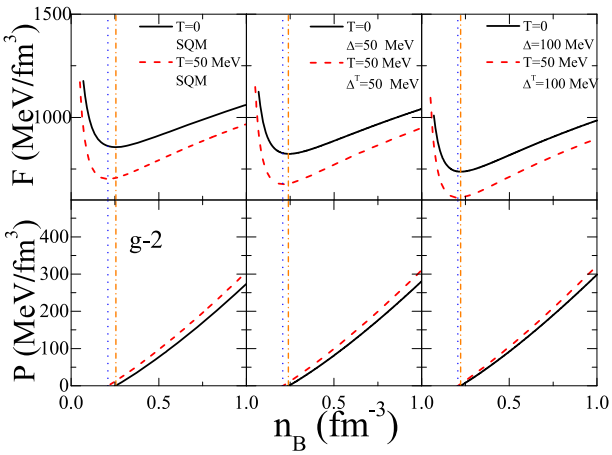

Fig. 1 Free energy per baryon and pressure as functions of baryon density with different nonvanishing common energy gap $\Delta(\Delta^T)$ at $T = 0$ and $T = 50$ MeV

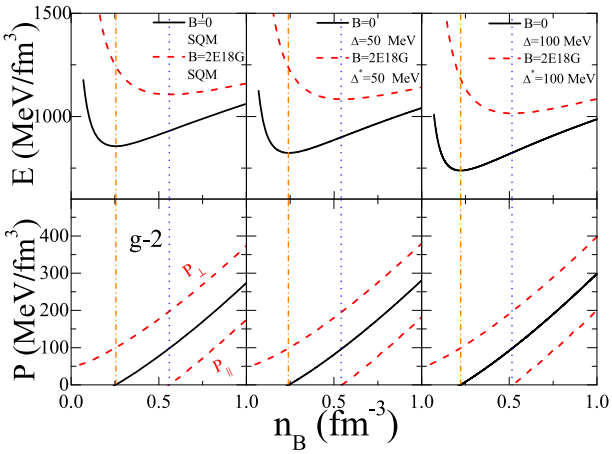

Fig. 2 Energy per baryon and anisotropic pressures as functions of baryon density with $\Delta^* = 50$ and $\Delta^* = 100$ MeV under constant magnetic field B

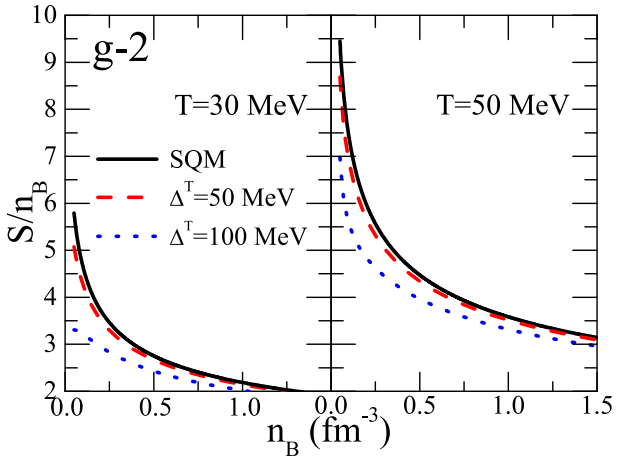

Fig. 3 Entropy per baryon as a function of baryon density at $T = 30$ MeV and $T = 50$ MeV with different Δ^T

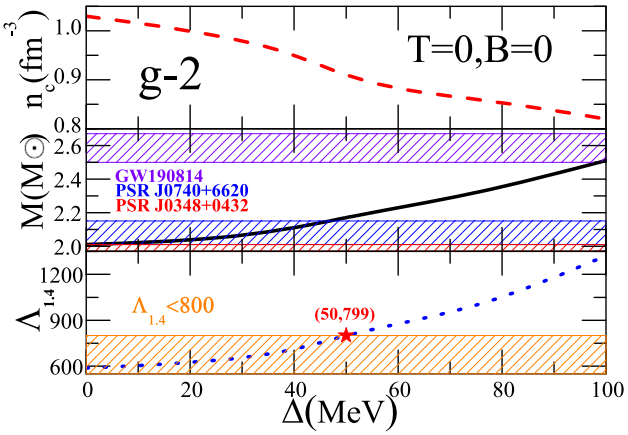

Fig. 4 Central density, maximum star mass, and tidal deformability of QSs with $g-2$ as functions of Δ at $T = 0$ and $B = 0$

One can find in Fig. 2 that the energy per baryon decreases with Δ^* while increasing with the magnetic field when n_B is fixed, which implies that the MCFL quark matter is more stable than the ordinary SQM in magnetic field case within quasiparticle model. Furthermore, it can also be seen that the zero longitudinal pressure density is identical with the baryon density of the minimum energy per baryon for MCFL quark matter under strong magnetic field to satisfy the thermodynamical self-consistency, and the difference between longitudinal pressure $P_\parallel$ and transverse pressure $P_\perp$ becomes very large when magnetic field B increases to $B = 2 \times 10^{18}$G. We then calculate the normalized pressure splitting factor $\delta_p = 2(p_\perp - p_\parallel)/(p_\perp + p_\parallel)$ to quantitatively describe the pressure anisotropy in MCFL quark matter under strong magnetic fields with different Δ in g-2, and we find $\delta_P = 0.72,\ 0.706,\ 0.65$ at $n_B = 1\text{fm}^{-3}$ in $B = 2 \times 10^{18}$G when $\Delta^* = 0,\ 50,\ 100$ MeV, which implies that the degree of the pressure anisotropy for MCFL quark matter under strong magnetic field can be reduced with the effective gap Δ^* within quasiparticle model.

In Fig. 3, we calculate the entropy per baryon as a function of baryon density at $T = 30$ MeV and $T = 50$ MeV for SQM and CFL quark matter cases. One can find that the entropy per baryon increases when temperature increases, while S/n_B decreasing with Δ^T, which implies that the degree of disorder for quark matter can be reduced at CFL case and increased at high temperature.

3.2 Properties of quark star and quark star matter

In the middle panel of Fig. 4, we calculate the maximum star mass as functions of Δ at zero temperature and zero magnetic field with g-2, and we also draw the secondary component m_2 of GW190814 with the mass of 2.50 $M_\odot$ − 2.67 $M_\odot$ at 90% credible level, the heavy pulsar PSR J0348+0432 with the mass of 2.01 ± 0.04 $M_\odot$, and the compact star PSR J0740+6620 with the mass of 2.08 ± 0.07 $M_\odot$ as the shaded area in the middle panel of Fig. 4. We can find the maximum star mass increases with Δ from 2.01 solar mass (SQM case) to 2.51 solar mass ($\Delta = 100$ MeV), which indicates that star matter for CFL phase can support much heavier quark stars than the star matter for SQM, and this conclusion matches the result in Fig. 1 that the pressure becomes larger at CFL phase than that in SQM at zero temperature. For the upper panel in this figure, we can find the central density of QSs decreases with Δ from $n_B = 1.03$ fm^{-3} (SQM case) to $n_B = 0.82$ fm^{-3} ($\Delta = 100$ MeV, CFL case), which implies that the average baryon density and the compactness of QSs might be reduced by considering CFL quark matter in the compact stars. Furthermore, we calculate the corresponding tidal deformability at 1.4 solar mass as a function of Δ in the lower panel, and the shaded area comes from the upper limit of $\Lambda_{1.4} < 800$ for the low-spin priors of the 1.4 solar mass pulsars in GW190817 [10]. One can find that $\Lambda_{1.4}$ increases with Δ and reaches the upper limit once $\Delta = 50$ MeV. Then our results indicate that the compact star comprising CFL quark matter may possess larger maximum star mass and tidal deformability ($\Lambda_{1.4}$), but the average star density might be reduced by CFL quark matter inside the stars.

In Fig. 5, we calculate the squared speed of sound as functions of the total energy density with $\Delta = 30 - 50$ MeV at $T = 0$ and $B = 0$, and we find that the sound speed for all cases is less than the speed of light, which satisfies the causality condition. Furthermore, one can find in Fig. 5 that the squared speed of sound increases with the energy density in $\Delta = 30,\ 35,\ 40$ MeV cases while decreasing with $\mathcal{E}_{tot}$ in $\Delta = 43,\ 45,\ 50$ MeV cases in g-2 within quasiparticle model. It is interesting to see that the squared speed of sound almost keeps the value as a constant 1/3 (which is exactly the so-called conformal limit of the squared speed of sound) with the energy density increasing in $\Delta = 42$ MeV case with g-2 within quasiparticle model.

For proto-neutron stars (PNSs) along the time evolution line, people usually describe the first minutes of life of PNSs by three snapshots with isentropic stages as

$$\text{(I)}\ \ S/n_B = 1,\ Y_l = 0.4, \tag{23}$$
$$\text{(II)}\ \ S/n_B = 2,\ Y_{\nu_l} = 0, \tag{24}$$
$$\text{(III)}\ \ S/n_B = 0,\ Y_{\nu_l} = 0, \tag{25}$$

where the entropy per baryon is set about one and the number of leptons per baryon with trapped neutrinos is about 0.4 ($Y_l = Y_e + Y_\mu + Y_{\nu_l} = Y_e + Y_\mu + Y_{\nu_e} + Y_{\nu_\mu} = 0.4$) for the 1st isentropic stage. In the following stage, the neutrinos diffuse and heat the star matter, which increase the corresponding entropy per baryon increasing to 2. Then in the 3rd stage, the temperature of the star decreases to zero and we can obtain the conventional neutron stars. On the other side, once we consider the star matter being CFL quark matter, the fraction of the leptons in the 1st isentropic stage should be zero, which is then not the proto-quark star (PQS) scenario. In this work, we still use the similar isentropic stages from PQSs to investigate the quark star mass at finite temperature within CFL quark phase, and we should mention that this scenario proposed is not the PQS scenario because there is no diffusing neutrinos to heating the star with CFL quark matter (we use the isentropic stages here mainly with the purpose of investigating the quark star mass at finite temperature within CFL quark phase). Then one can rewrite the isentropic stages for the QSs at finite temperature within CFL quark phase as

$$\text{(I)}\ \ S/n_B = 1\ ,\ Y_l = 0, \tag{26}$$
$$\text{(II)}\ \ S/n_B = 2\ ,\ Y_l = 0, \tag{27}$$
$$\text{(III)}\ \ S/n_B = 0\ ,\ Y_l = 0. \tag{28}$$

In Fig. 6, we calculate the mass-radius relation at different isentropic stages of quark stars for CFL quark matter phase with $\Delta^T = 50$ MeV and $\Delta^T = 100$ MeV. One can find in Fig. 6 that the maximum quark star mass in $\Delta = 50$ MeV case increases from 2.17 $M_\odot$ for $T = 0$ to 2.19 $M_\odot$ for $S/n_B = 1$, and the maximum star mass can finally increase to 2.23 $M_\odot$ for $S/n_B = 2$. In $\Delta = 100^T$ MeV case, the maximum quark star mass becomes even larger at corresponding isentropic stages, where the maximum mass for quark stars are 2.51 $M_\odot$, 2.58 $M_\odot$, and 2.65 $M_\odot$ for $T = 0$, $S/n_B = 1$, and $S/n_B = 2$ respectively. Our results indicate that the maximum mass of QSs for CFL quark matter increases with the entropy per baryon in the isentropic stages and the maximum star mass also increases with Δ^T at finite temperature.

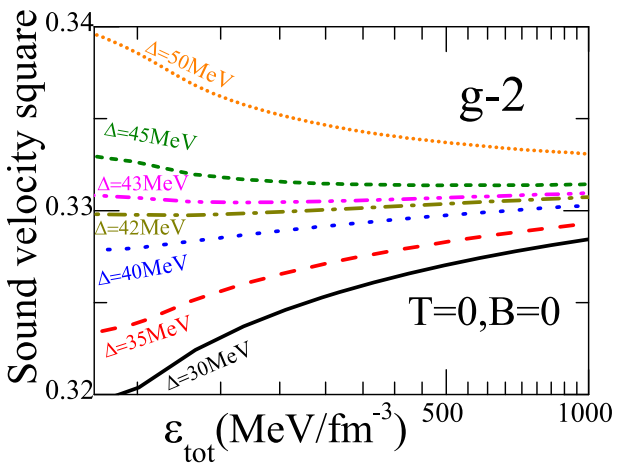

Fig. 5 Sound velocity square as functions of the total energy density with different Δ at $T = 0$ and $B = 0$

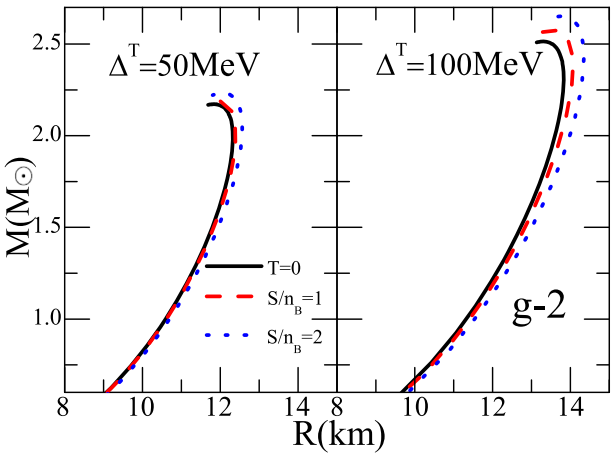

Fig. 6 Mass-radius relation at different isentropic stages of quark stars with different Δ^T

In Fig. 7, we show the core temperature T_c (here the core temperature means the temperature at the center of the star for the maximum mass case) and 1.4 $M_\odot$ temperature $T_{1.4}$ of QSs for CFL quark matter at $S/n_B = 1$ and $S/n_B = 2$ stages as functions of baryon density with $\Delta^T = 50$ MeV and $\Delta^T = 100$ MeV. One can find from Fig. 7 that both T_c and $T_{1.4}$ increase with the increment of the entropy per baryon with $\Delta^T = 50$ MeV and $\Delta^T = 100$ MeV, and both T_c and $T_{1.4}$ also increase with Δ^T at a certain S/n_B. One can also find in Fig. 7 that the central density of the maximum mass of QSs decreases with both S/n_B and Δ^T. Our results indicate that both the entropy per baryon S/n_B and Δ^T can significantly influence the EOS, the maximum mass, and the core temperature of the QSs made up of CFL quark matter.

In Fig. 8, we calculate the mass-radius lines of QSs in SQM and CFL phase within quasiparticle model. The gray shaded region with $R = 13.7^{+2.6}_{-1.5}$ km and $M = 2.08 \pm 0.07$ $M_\odot$ shows the mass-radius constraint of PSR J0740+6620 from [9], the dark cyan shaded region with $R = 13.02^{+1.24}_{-1.06}$ km and $M = 1.44^{+0.15}_{-0.14}$ $M_\odot$ is the measurement of PSR J0030+0451 [106], the pink shaded region with $R = 10.4^{+0.86}_{-0.78}$ km and $M = 0.77^{+0.20}_{-0.17}$ $M_\odot$ comes from the estimate from the central compact object within the supernova remnant HESS J1731-347 [107], and the wine shaded region for 4U 1702-429 [108]

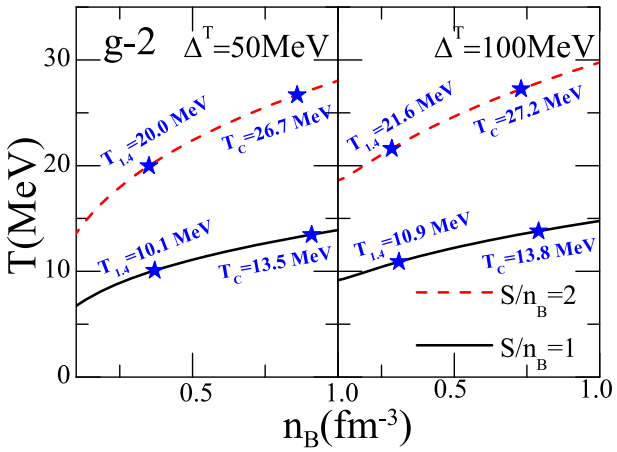

Fig. 7 Core temperature and 1.4 $M_\odot$ temperature at different isentropic stages of quark stars with as functions of baryon density with different Δ^T

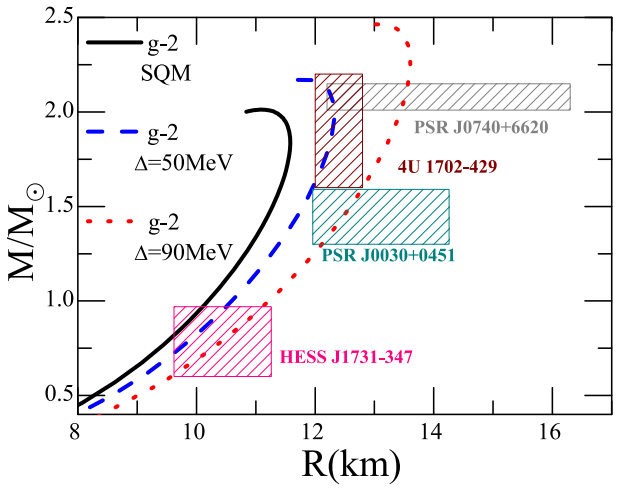

Fig. 8 Mass-radius lines of QSs in SQM and CFL phase within quasiparticle model

estimates $R = 12.4 \pm 0.4$ km and $M = 1.9 \pm 0.3\ M_\odot$. One can see in Fig. 8 that the mass-radius line of g-2 in SQM with the maximum star mass being 2.01 $M_\odot$ only satisfies the constraint of the estimate from HESS J1731-347 [107]. For g-2 $\Delta = 50$ MeV case, we find the mass-radius line can satisfy all the mass-radius constraints in Fig. 8 (which exactly reaches the left boundary of the estimate region of PSR J0030+0451), and the tidal deformability $\Lambda_{1.4}$ is calculated as 799, which reaches the upper limit of $\Lambda_{1.4} < 800$ for the low-spin priors of the pulsars in GW170817. For g-2 $\Delta = 90$ MeV case, one can find the mass-radius line also satisfies all the listed mass-radius constraints, which reaches exactly the right boundary of the region of 4U 1702-429. Furthermore, the tidal deformability for g-2 $\Delta = 90$ MeV case is calculated as $\Lambda_{1.4} = 1201$, which cannot satisfy the the upper limit of $\Lambda_{1.4} < 800$ for the pulsars in GW170817. Then our results indicate that we can provide the large QSs within CFL quark phase from quasiparticle model by satisfying both the upper limit of $\Lambda_{1.4} < 800$ for the low-spin priors of 1.4 solar mass pulsars from GW170817 and the new estimates of the mass-radius region from PSR J0740 + 6620, PSR J0030 + 0451, HESS J1731-347, and 4U 1702-429, which cannot be obtained by considering the QSs with SQM within quasiparticle model.

4 Conclusion and discussion

In this work, we explore the thermodynamical properties of CFL quark matter in quark stars at zero temperature case, finite temperature cases, and strong magnetic field case. The EOS of CFL quark matter, the entropy per baryon, the sound speed, the central density and core temperature, and the maximum mass of QSs are also studied by using quark quasiparticle model.

We first investigate the thermodynamical properties of CFL quark matter. Our results indicate that we can obtain more stable CFL quark matter by considering large nonvanishing common gap in quark phase, and the EOS of CFL quark matter becomes stiffer with Δ at zero temperature case, finite temperature cases, and strong magnetic field case. We have further calculated the entropy per baryon of CFL quark matter at finite temperature, and the result shows that the entropy per baryon decreases with Δ^T, which implies that the degree of disorder for quark matter can be reduced at CFL case and increased at high temperature.

Furthermore, we calculate the maximum star mass, $\Lambda_{1.4}$, and the central density of the quark stars for CFL quark matter at zero temperature as functions of Δ. The results indicate that both $\Lambda_{1.4}$ and the maximum star mass increase with Δ because of the EOS for CFL phase being stiffer with the energy gap, while the average star density might be reduced by considering CFL quark matter inside the star due to the decrement of the central density of QSs by considering Δ.

For the properties of QSs at finite temperature, we calculate the mass-radius relation at different isentropic stages of QSs for CFL star matter at finite temperature, and we find that both the entropy per baryon of the isentropic stages and Δ^T can significantly influence the EOS, the maximum mass, and the core temperature of the QSs made up of CFL quark matter.

Therefore, our results have demonstrated that considering CFL quark matter can significantly change the EOS of quark matter as well as the properties of CFL quark matter in QSs at zero temperature, finite temperature, and strong magnetic field. In particular, our results have shown that CFL quark matter may be more stable than SQM and can support more massive QSs at zero temperature and finite temperature. Moreover, we can provide the large QSs within CFL quark phase from quasiparticle model by satisfying both the

upper limit of $\Lambda_{1.4} < 800$ for the low-spin priors of 1.4 solar mass pulsars from GW170817 and the new estimates of the mass-radius region from PSR J0740 + 6620, PSR J0030 + 0451, HESS J1731-347, and 4U 1702-429, which cannot be obtained by considering the QSs with SQM within quasiparticle model.

Acknowledgements This work is supported by the NSFC under Grants No. 11975132, 12205158, 12305148, and 11505100, and the Shandong Provincial Natural Science Foundation, China ZR2022JQ04, ZR2021QA037, ZR2019YQ01 and ZR2015AQ007.

Data Availability Statement This manuscript has no associated data or the data will not be deposited. [Authors' comment: This is a theoretical study and no experimental data has been listed].

Funded by SCOAP[3]. SCOAP[3] supports the goals of the International Year of Basic Sciences for Sustainable Development.

References

1. N.K. Glendenning, *Compact Stars*, 2nd edn. (Spinger, New York, 2000)
2. F. Weber, *Pulsars as Astrophyical Laboratories for Nuclear and Particle Physics* (IOP Publishing Ltd, London, 1999)
3. J.M. Lattimer, M. Prakash, Science **304**, 536 (2004)
4. A.W. Steiner, M. Prakash, J.M. Lattimer, P.J. Ellis, Phys. Rep. **410**, 325 (2005)
5. P. Demorest, Nature **467**, 1081 (2010)
6. J. Antoniadis et al., Science **340**, 6131 (2013)
7. H. Thankful Cromartie et al., Nat. Astron. Lett. (2019). arXiv:1904.06759
8. E. Fonseca et al., Astrophys. J. Lett. **915**, L12 (2021)
9. M.C. Miller et al., Astrophys. J. Lett. **918**, L28 (2021)
10. B.P. Abbott et al., Phys. Rev. Lett. **119**, 161101 (2017)
11. R. Abbott et al., Astrophys. J. Lett. **896**, L44 (2020)
12. D. Ivanenko, D.F. Kurdgelaidze, Lett. Nuovo Cimento **2**, 13 (1969)
13. N. Itoh, Prog. Theor. Phys. **44**, 291 (1970)
14. A.R. Bodmer, Phys. Rev. D **4**, 1601 (1971)
15. E. Witten, Phys. Rev. D **30**, 272 (1984)
16. E. Farhi, R.L. Jaffe, Phys. Rev. D **30**, 2379 (1984)
17. C. Alcock, E. Farhi, A. Olinto, Astrophys. J. **310**, 261 (1986)
18. F. Weber, Prog. Part. Nucl. Phys. **54**, 193 (2005)
19. I. Bombaci, I. Parenti, I. Vidana, Astrophys. J. **614**, 314 (2004)
20. J. Staff, R. Ouyed, M. Bagchi, Astrophys. J. **667**, 340 (2007)
21. M. Herzog, F.K. Röpke, Phys. Rev. D **84**, 083002 (2011)
22. M.A. Stephanov, K. Rajagopal, E.V. Shuryak, Phys. Rev. Lett. **81**, 4816 (1998)
23. H. Terazawa, INS-Report 336, Univ. of Tokyo (1979)
24. P.C. Chu et al., EPJC **81**, 569 (2021)
25. M. Alford, S. Reddy, Phys. Rev. D **67**, 074024 (2003)
26. M. Alford, P. Jotwani, C. Kouvaris, J. Kundu, K. Rajagopal, Phys. Rev. D **71**, 114011 (2005)
27. M. Baldo, Phys. Lett. B **562**, 153 (2003)
28. N.D. Ippolito, M. Ruggieri, D.H. Rischke, A. Sedrakian, F. Weber, Phys. Rev. D **77**, 023004 (2008)
29. X.Y. Lai, R.X. Xu, Res. Astron. Astrophys. **11**, 687 (2011)
30. M.G.B. de Avellar, J.E. Horvath, L. Paulucci, Phys. Rev. D **84**, 043004 (2011)
31. L. Bonanno, A. Sedrakian, A&A **539**, A16 (2012)
32. P.C. Chu et al., Phys. Rev. D **94**, 123014 (2016)
33. P.C. Chu et al., Eur. Phys. J. C **77**, 512 (2017)
34. P.C. Chu et al., J. Phys. G Nucl. Part. Phys. **47**, 085201 (2020)
35. D. Bailin, A. Love, Phys. Rep. **107**, 325 (1984)
36. M.G. Alford, K. Rajagopal, S. Reddy, F. Wilczek, PRD **64**, 074017 (2001)
37. I.A. Shovkovy, Found. Phys. **35**, 1309 (2005)
38. K. Rajagopal, F. Wilczek, Phys. Rev. L **86**, 3492–3495 (2001)
39. M.G. Alford, K. Rajagopal, T. Schaefer, A. Schmitt, Rev. Mod. Phys. **80**, 1455 (2008)
40. G. Lugones, J.E. Horvath, Astron. Astrophys. **403**, 173 (2003)
41. J.E. Horvath, G. Lugones, Astron. Astrophys. **422**, L1 (2004)
42. P.C. Chu, L.W. Chen, X. Wang, Phys. Rev. D **90**, 063013 (2014)
43. P.C. Chu et al., Phys. Rev. C **99**, 035802 (2019)
44. P.C. Chu et al., Phys. Rev. D **100**, 103012 (2019)
45. P.C. Chu et al., Eur. Phys. J. C **81**, 93 (2021)
46. A. Chodos, R.L. Jaffe, K. Ohnson, C.B. Thorn, V.F. Weisskopf, Phys. Rev. D **9**, 3471 (1974)
47. M. Alford, M. Braby, M. Paris, S. Reddy, Astrophys. J. **629**, 969 (2005)
48. J.Y. Chao et al., Phys. Rev. D **88**, 054009 (2013)
49. P.C. Chu et al., Phys. Rev. D **91**, 023003 (2015)
50. P.C. Chu et al., Phys. Rev. D **93**, 094032 (2016)
51. P.C. Chu et al., Phys. Rev. D **96**, 083019 (2017)
52. P. Rehberg, S.P. Klevansky, J. Hüfner, Phys. Rev. C **53**, 410 (1996)
53. M. Hanauske, L.M. Satarov, I.N. Mishustin, H. Stocker, W. Greiner, Phys. Rev. D **64**, 043005 (2001)
54. S.B. Rüster, D.H. Rischke, Phys. Rev. D **69**, 045011 (2004)
55. D.P. Menezes, C. Providencia, D.B. Melrose, J. Phys. G **32**, 1081 (2006)
56. C.D. Roberts, A.G. Williams, Prog. Part. Nucl. Phys. **33**, 477 (1994). (**and references therein**)
57. H.S. Zong, L. Chang, F.Y. Hou, W.M. Sun, Y.X. Liu, Phys. Rev. C **71**, 015205 (2005)
58. S.X. Qin, L. Chang, H. Chen, Y.X. Liu, C.D. Roberts, Phys. Rev. Lett. **106**, 172301 (2011)
59. B.A. Freedman, L.D. Mclerran, Phys. Rev. D **16**, 1169 (1977)
60. E.S. Fraga, R.D. Pisarski, J. Schaffner-Bielich, Phys. Rev. D **63**, 121702(R) (2001)
61. E.S. Fraga, P. Romatschke, Phys. Rev. D **71**, 105014 (2005)
62. A. Kurkela, P. Romatschke, A. Vuorinen, Phys. Rev. D **81**, 105021 (2010)
63. G.N. Fowler, S. Raha, R.M. Weiner, Z. Phys. C **9**, 271 (1981)
64. S. Chakrabarty, S. Raha, B. Sinha, Phys. Lett. B **229**, 112 (1989)
65. S. Chakrabarty, Phys. Rev. D **43**, 627 (1991)
66. S. Chakrabarty, Phys. Rev. D **48**, 1409 (1993)
67. S. Chakrabarty, Phys. Rev. D **54**, 1306 (1996)
68. O.G. Benvenuto, G. Lugones, Phys. Rev. D **51**, 1989 (1995)
69. G.X. Peng, H.C. Chiang, J.J. Yang, L. Li, B. Liu, Phys. Rev. C **61**, 015201 (1999)
70. G.X. Peng, H.C. Chiang, B.S. Zou, P.Z. Ning, S.J. Luo, Phys. Rev. C **62**, 025801 (2000)
71. G.X. Peng, A. Li, U. Lombardo, Phys. Rev. C **77**, 065807 (2008)
72. A. Li, G.X. Peng, J.F. Lu, Res. Astron. Astrophys. **11**, 482 (2011)

73. K. Schertler, C. Greiner, M.H. Thoma, Nucl. Phys. A **616**, 659 (1997)
74. K. Schertler, C. Greiner, P.K. Sahu, M.H. Thoma, Nucl. Phys. A **637**, 451 (1998)
75. P.C. Chu, L.W. Chen, Astrophys. J. **780**, 135 (2014)
76. P.C. Chu et al., Phys. Lett. B **778**, 447 (2018)
77. P.C. Chu, L.W. Chen, Phys. Rev. D **96**, 103001 (2017)
78. D.T. Son, M.A. Stephanov, Phys. Rev. L **86**, 592 (2001)
79. M. Frank, M. Buballab, M. Oertel, Phys. Lett. B **562**, 221 (2003)
80. D. Toublan, J.B. Kogut, Phys. Lett. B **564**, 212 (2003)
81. J.B. Kogut, D.K. Sinclair, Phys. Rev. D **70**, 094501 (2004)
82. L. He, M. Jin, P. Zhuang, Phys. Rev. D **71**, 116001 (2005)
83. L. He, P. Zhuang, PLB **615**, 93 (2005)
84. M. Di Toro, A. Drago, T. Gaitanos, V. Greco, A. Lavagno, NPA **775**, 102 (2006)
85. Z. Zhang, Y.X. Liu, Phys. Rev. C **75**, 064910 (2007)
86. G. Pagliara, J. Schaffner-Bielich, PRD **81**, 094024 (2010)
87. G.Y. Shao et al., Phys. Rev. D **85**, 114017 (2012)
88. P.C. Chu et al., Phys. Rev. C **105**, 045806 (2022)
89. H. Liu et al., Phys. Rev. D **105**, 043015 (2022)
90. Y.N. Wang et al., Acta Phys. Sin. **71**(22), 222101 (2022)
91. K. Schertler, C. Greiner, M.H. Thoma, Nucl. Phys. A **616**, 659 (1997)
92. R.D. Pisarski, Nucl. Phys. A **498**, 423 (1989)
93. X.J. Wen et al., J. Phys. G Nucl. Part. Phys. **36**, 025011 (2009)
94. Z. Zhang et al., Phys. Rev. D **103**, 103021 (2021)
95. B.K. Patra, C.P. Singh, Phys. Rev. D **54**, 3551 (1996)
96. L. Paulucci, J.E. Horvath, Phys. Rev. C **78**, 064907 (2008)
97. E.J. Ferrer, Vivian de la Incera, Phys. Rev. Lett. **95**, 152002 (2005)
98. E.J. Ferrer, V. de la Incera, C. Manuel. Nucl. Phys. B **747**, 88–112 (2006)
99. B. Feng, E.J. Ferrer, Vivian de la Incera, Nucl. Phys. B **853**, 213–239 (2011)
100. L. Paulucci, Efrain J. Ferrer, Vivian de la Incera, J.E. Horvath, Phys. Rev. D **83**, 043009 (2011)
101. A.A. Isayev, J. Yang, J. Phys. G **40**, 035105 (2013)
102. D. Bandyopadhyay, S. Chakrabarty, S. Pal, Phys. Rev. Lett. **79**, 2176 (1997)
103. D. Bandyopadhyay, S. Pal, S. Chakrabarty, J. Phys. G **24**, 1647 (1998)
104. E.J. Ferrer, V. de la Incera, J.P. Keith, I. Portillo, P.L. Springsteen, Phys. Rev. C **82**, 065802 (2010)
105. E.J. Ferrer, V. de la Incera, Lect. Notes Phys. **871**, 399 (2013)
106. M.C. Miller et al., Astrophys. J. Lett. **887**, L24 (2019). (**(28pp)**)
107. V. Doroshenko, V. Suleimanov, G. Phlhofer, A. Santangelo, Nat. Astron. **6**, 1444 (2022)
108. J. Nattila et al., A&A **608**, A31 (2017)